Angewandte Chemie International Edition

Angewandte International Edition Chemie

GDCh German Chemical Society

How to cite: *Angew. Chem. Int. Ed.* **2026**, 65, e8986387
doi.org/10.1002/anie.8986387

COMMUNICATION

Circumstellar Origin of Chrysene ($C_{18}H_{12}$) via Self-Recombination of Resonantly-Stabilized 1-Indenyl Radicals and Implications to the Aromaticity of the Carbonaceous Asteroid Ryugu

Souvick Biswas[1] | Shane J. Goettl[1] | Vladislav S. Krasnoukhov[2] | Nureshan Dias[3] | Valeriy N. Azyazov[2] | Sabrina Arias[4] | Stanislaw F. Wnuk[4] | Musahid Ahmed[3] | Alexander M. Mebel[4] | Ralf I. Kaiser[1]

[1]Department of Chemistry, University of Hawai'i at Manoa, Honolulu, Hawaii, USA | [2]Samara National Research University, Samara, Russian Federation | [3]Chemical Sciences Division, Lawrence Berkeley National Laboratory, Berkeley, California, USA | [4]Department of Chemistry and Biochemistry, Florida International University, Miami, Florida, USA

Correspondence: Musahid Ahmed (mahmed@lbl.gov) | Alexander M. Mebel (mebela@fiu.edu) | Ralf I. Kaiser (ralfk@hawaii.edu)

Received: 2 January 2026 | **Revised:** 8 April 2026 | **Accepted:** 15 April 2026

Keywords: gas-phase reactions | polycyclic aromatic hydrocarbon | reaction mechanisms | ring expansion | spiro-intermediates

ABSTRACT

Polycyclic aromatic hydrocarbons (PAHs) represent key molecular building blocks of carbonaceous nanoparticles and have been identified in cold molecular clouds (TMC-1), meteorites (Murchison, Allende), and asteroids (Bennu, Ryugu). However, the understanding of their formation and molecular mass growth processes in these extreme environments has remained elusive, especially with the emergence of resonantly-stabilized free radical (RSFR)-mediated pathways. Here, we report a combined experimental and computational study on the self-recombination of the aromatic and resonantly-stabilized 1-indenyl radical ($C_9H_7^{\bullet}$) isomer-selectively forming the 18π-Hückel PAH chrysene ($C_{18}H_{12}$) in an overall endoergic reaction. These features account for the circumstellar origin of chrysene in pristine samples of the carbonaceous asteroid Ryugu and of the Murchison meteorite. At the microscopic level, the ring expansion involving cyclopentadienyl moieties to two six-membered aromatic rings via pivotal spiroaromatic intermediates affords a versatile, RSFR-initiated mass growth channel essentially leading to graphene-type PAHs and eventually two-dimensional nanostructures in high temperature circumstellar envelopes and in combustion processes.

Polycyclic aromatic hydrocarbons (PAHs)—organic molecules composed of fused benzene rings have emerged as the missing link between small carbon molecules and carbonaceous nanoparticles (interstellar grains) [1] encompassing up to 30% of the galactic carbon budget [2, 3]. Very recently, pristine samples from the near-Earth carbonaceous asteroid Ryugu were collected by the Hayabusa2 spacecraft and revealed a pool of aromatics with up to 61 carbon atoms [4–6]. Carbonaceous asteroids like Ryugu and Bennu represent a key class of asteroids which are rich in carbon and make up some 75% of all known asteroids in our solar system [7]. These asteroids are some of the oldest objects in our solar system and are largely unchanged since their formation over 4.5 billion years ago from the accretion of interstellar material (10 K) and dust processed in circumstellar envelopes at temperatures of a few 1000 K [8–12]. Therefore, an understanding of the origin and formation pathways of PAHs of these asteroids can offer detailed insights into the chemical evolution and origin of organic material in the early solar system. Sophisticated ^{13}C isotope analyses of PAHs emerged as key indicators and benchmarks to elucidate the physical conditions of the origin of aromatics in deep space. In Ryugu's samples, aromatics such as pyrene ($C_{16}H_{10}$) and fluoranthene ($C_{16}H_{10}$) were revealed

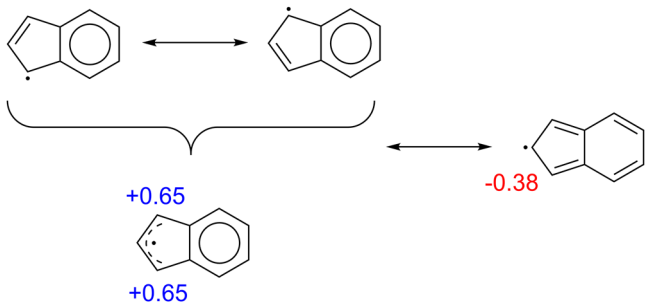

SCHEME 1 | Resonantly stabilized 1-indenyl ($C_9H_7^{\bullet}$) radical [27].

to originate from cold molecular clouds, while PAHs such as phenanthrene ($C_{14}H_{10}$) and anthracene ($C_{14}H_{10}$) were inferred to originate from high temperature regions of circumstellar envelopes [13]. Similarly, PAHs in carbonaceous chondrites such as Murchison, Allende, and Orgueil [14, 15] are linked to high temperature circumstellar origins of aromatics in carbon-rich asymptotic giant branch (AGB) stars and planetary nebulae as their descendants [16].

However, a fundamental understanding of molecular mass growth processes leading to aromatics is still in its infancy. Contemporary astrochemical models rely on hydrogen abstraction–carbon addition (HACA) mechanisms, which involve repetitive sequences of atomic hydrogen abstractions from an aromatic hydrocarbon like benzene followed by consecutive addition of one or two acetylene molecule(s) prior to cyclization and aromatization [17]. However, in deep space, PAHs get destroyed by photolysis, galactic cosmic rays, and shock waves resulting in lifetimes of a few 10^8 years, which are significantly shorter than those timescales modeled for an injection of PAHs from carbon rich AGB stars of a few 10^9 years [18]. Hence, PAHs are not expected to exist in the interstellar medium or survive to accrete in carbonaceous asteroids such as Ryugu. Nevertheless, the ubiquitous presence of such species, especially in carbonaceous asteroids and meteorites, suggests elusive high-temperature routes for the rapid growth of PAHs in circumstellar envelopes of carbon rich stars. From the mechanistic viewpoint, resonantly stabilized free radicals (RSFRs) - organic open-shell transients, such as propargyl ($C_3H_3^{\bullet}$), allyl ($C_3H_5^{\bullet}$), cyclopentadienyl ($C_5H_5^{\bullet}$), and 1-indenyl ($C_9H_7^{\bullet}$), in which the unpaired electron is delocalized over the carbon skeleton, have emerged as fundamental molecular building blocks to PAHs in high temperature environments such as combustion flames and in circumstellar envelopes [19–25]. In particular, aromatic and RSFR 1-indenyl ($C_9H_7^{\bullet}$) radical (Scheme 1) constitutes the elementary unit of non-planar PAHs such as corannulene ($C_{20}H_{10}$), nanobowls ($C_{40}H_{10}$), and fullerenes (C_{60} and C_{70}), where the five-membered ring curves the carbon skeleton out of the planar geometry [26–28]. However, in general the molecular mass growth processes of RSFRs leading to even small-sized planar PAHs carrying three aromatic rings (e.g. anthracene, phenanthrene) or more have remained elusive [29].

Here, we report a combined experimental and computational study on the self-recombination of the 1-indenyl radical ($C_9H_7^{\bullet}$) synthesizing prototype 18π Hückel-aromatic system, chrysene ($C_{18}H_{12}$) as simple representative of a key class of PAHs–phenacenes–carrying benzene rings fused in a zigzag structure. The 1-indenyl radical is generated in situ by selected carbon-bromine bond cleavage of the helium seeded 1-bromoindene (C_9H_7Br) precursor within a chemical microreactor (Supporting Information S1) [30]. A residence time of some 100 μs in the reactor was chosen to focus on the initial stages of the molecular mass growth between two indenyl radicals thus eliminating further growth reactions with 1-indenyl radicals that could complicate the interpretation of synchrotron-based molecular beam photoionization mass spectrometry data on the fundamental bond-formation processes. Electronic structure calculations reveal that chrysene forms at high temperatures through ring expansion involving pivotal spiroaromatic intermediates. Together with molecular beam studies, these results elucidate the high-temperature origin of chrysene ($C_{18}H_{12}$) detected on the carbonaceous asteroid Ryugu. Notably, among the PAHs identified by laser desorption–laser multiphoton ionization mass spectrometry (L_2MS) [4], $C_{18}H_{12}$ species are among the most abundant aromatics detected in the return samples from Ryugu, providing key insights into the chemical evolution and origins of organic, aromatic matter in the early Solar System.

Mass Spectra and Photoionization Efficiency Curves: A representative mass spectrum recorded at a photon energy of 9.50 eV is displayed in Figure 1a for the self-reaction of the 1-indenyl radical ($C_9H_7^{\bullet}$; 115 amu) formed via flash pyrolysis of 1-bromoindene [$C_9H_7{}^{79}Br$ (194 amu), $C_9H_7{}^{81}Br$ (196 amu)]. Considering reactions of the primary reactant (1-indenyl radical), multiple peaks appear at higher mass-to-charge ratios (m/z) as the result of distinct molecular mass growth processes. Major peaks at m/z = 116, 128, 152, 154, 176, 178, 180, 228, 229, and 230 are identified (Figure 1, Figures S1–S3); these can be linked to hydrocarbons of the molecular formulae C_9H_8, $C_{10}H_8$, $C_{12}H_8$, $C_{12}H_{10}$, $C_{14}H_8$, $C_{14}H_{10}$, $C_{14}H_{12}$, $C_{18}H_{12}$, $^{13}C_{18}H_{12}/C_{18}H_{13}$, and $C_{18}H_{14}$. For an isomer-specific assignment of these species, photoionization efficiency (PIE) curves are recorded at individual m/z peaks by scanning the photon energy in 0.05 eV steps in the range from 7.3 to 10.0 eV while simultaneously recording the ion count normalized to the photocurrent [31–33]. It is important to note that structural isomers, despite sharing the same formula, exhibit distinct PIE curves, enabling their identification [34]. The signal at m/z = 230 represents the self-recombination adduct ($C_{18}H_{14}$) of 1-indenyl radicals ($C_9H_7^{\bullet}$) (Reaction (1)). Under single-collision conditions, such as in crossed-beam experiments [35], the reaction adducts quickly break apart into the original reactants since the collision complex cannot dissipate the excess internal energy under single collision conditions. In contrast, within the chemical microreactor, collisions with helium atoms can remove some of this energy by transferring internal energy into the kinetic energy of the helium seeding gas, allowing a fraction of the $C_{18}H_{14}$ adducts to stabilize as products [36]. Alternatively, the energized $C_{18}H_{14}$ species can lose two hydrogen atoms in sequence, forming $C_{18}H_{12}$ species (228 amu) via Reaction (2). An analysis of the corresponding PIE curve at m/z = 228 reveals that this graph could be reproduced with the reference PIE curve of chrysene only (blue; Figure 1b). Another possible isomer [4]-helicene, with similar adiabatic ionization energy of 7.55 ± 0.05 eV may have some contribution to the experimental PIE curve alongside chrysene (Figure S4). However, based on the computed reaction energetics, the dominant formation of [4]-helicene is energetically unfavorable compared to that of

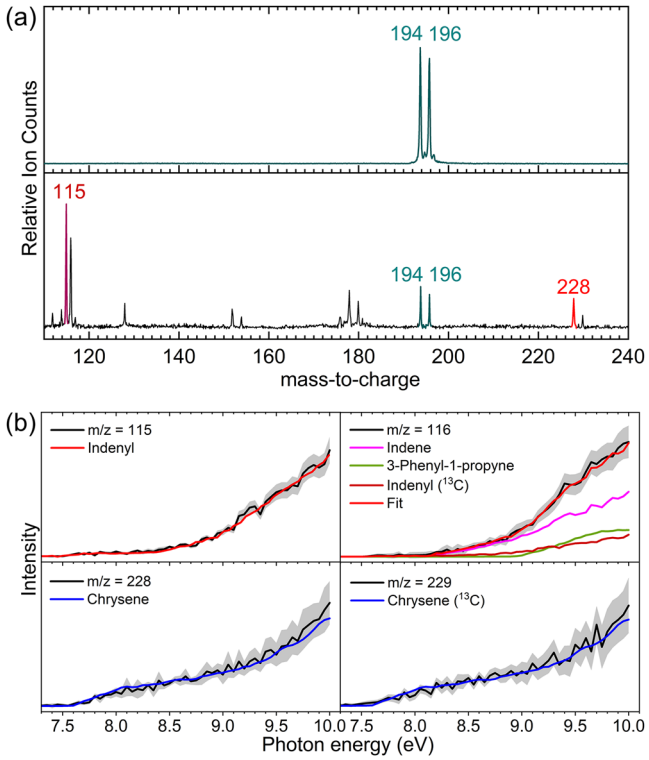

FIGURE 1 | (a) Photoionization mass spectra recorded at a photon energy of 9.50 eV for the precursor 1-bromoindene at a temperature of 298 K (upper panel) and indenyl ($C_9H_7^{\bullet}$) radical self-reaction at 1223 ± 20 K (bottom panel). (b) Photoionization efficiency (PIE) curves for relevant mass-to-charge (m/z = 115, 116, 228 and 229) peaks. Black: experimental PIE curves; blue/green/red/pink/orange: reference PIE curves. In case of multiple contributions to one PIE curve, the red line represents the overall fit. The error bars consist of two parts: ±10% based on the accuracy of the photodiode and a 1-σ error of the PIE curve averaged over the individual scans.

chrysene. Further, signal at m/z = 229 represents the ^{13}C isomer of m/z = 228; the corresponding PIE curve can also be fit with chrysene replicating the parent signal.

Having identified signal at m/z = 230, 229, and 228 as the result of molecular mass growth processes of the indenyl radical self-reaction, we briefly discuss the nature of the hydrocarbon observed via ion signals from m/z = 116 to 180. Since the 1-indenyl radical ($C_9H_7^{\bullet}$) can also be pyrolyzed in the chemical microreactor and hence decomposes to smaller hydrocarbon fragments such as propargyl ($C_3H_3^{\bullet}$), cyclopentadienyl ($C_5H_5^{\bullet}$), benzene (C_6H_6) [33], these fragments may also react with the 1-indenyl ($C_9H_7^{\bullet}$) radical (Figure S2, Table S1) [33, 37]. For instance, indene (C_9H_8), 3-phenyl-1-propyne (C_9H_8), and a contribution from the ^{13}C-indenyl radical ($^{13}C_9H_7^{\bullet}$) can be identified for m/z = 116 (Figure 1b) [28, 38–40]. Naphthalene ($C_{10}H_8$; 128 amu), biphenyl ($C_{12}H_{10}$; 154 amu), anthracene ($C_{14}H_{10}$; 178 amu), phenanthrene ($C_{14}H_{10}$; 178 amu), and (E)-stilbene ($C_{14}H_{12}$; 180 amu) are also notable (Table S1) [38, 19].

$$C_9H_7^{\bullet}\ (115\ \text{amu}) + C_9H_7^{\bullet}\ (115\ \text{amu}) \rightarrow C_{18}H_{14}\ \ (230\ \text{amu}) \quad (1)$$

$$C_{18}H_{14}\ \ (230\ \text{amu}) \rightarrow C_{18}H_{12}\ \ (228\ \text{amu}) + 2H\ (1\ \text{amu}) \quad (2)$$

Reaction Mechanism: With experimental evidence of the formation of chrysene ($C_{18}H_{12}$) through the gas-phase self-recombination of the 1-indenyl radical ($C_9H_7^{\bullet}$), our objective is to unravel the detailed reaction mechanisms. To interpret this complex process, electronic structure calculations of the relevant potential energy surfaces (PES) were performed to trace the feasible synthetic pathways (Figure 2). These calculations were conducted at the G3(MP2, CC)//B3LYP/6-311G(d, p) level of theory. Initially, two 1-indenyl radicals barrier-lessly recombine to form di-indene (5,6,7,7a-tetrahydro-1*H*,1′*H*-1,1-biindene; $C_{18}H_{14}$; **i1**) via carbon-carbon coupling at their C1 radical centers. This collision complex, which was detected experimentally via a signal at m/z = 230, is stabilized by 184 kJmol^{-1} with respect to the separated reactants and can lose a hydrogen atom from one of the C1 atoms of the indenyl moieties in an overall endoergic reaction (283 kJmol^{-1}) to generate the **i2** radical (1*H*,1′*H*-[1,1′-biinden]-1-yl radical; $C_{18}H_{13}^{\bullet}$).

In principle, **i2** can be also produced via a direct hydrogen atom abstraction, if their concentration in the reactor is sufficient to participate in the reactions, e.g., H + **i1** → **i2** + H_2 to compete with the unimolecular hydrogen atom loss from **i1**. We do not expect this to be the case at our experimental conditions since hydrogen atoms are not produced directly in the pyrolysis of bromoindene, whereas the produced bromine atoms are inefficient hydrogen atom abstractors since the H–Br bond is weaker than the C—H bond by 50 kJmol^{-1}. This **i2** radical represents the entry point accessing six distinct $C_{18}H_{12}$ isomers via extensive isomerization terminated by yet another hydrogen atom loss.

In detail, following the energetically most favorable isomerization, **i2** undergoes cyclization by accessing a three-membered fused ring (**i3**) followed by ring expansion to the exotic spiro-intermediate, the 3′*H*-spiro[indene-1,2′-naphthalene]-3′-yl radical (**i4**, 108 kJmol^{-1}) via a transition state located 69 kJmol^{-1} above **i3**. Upon cyclization, the spiro-intermediate **i4** forms a fused three-membered ring in intermediate **i5**; subsequent ring expansion generates a naphthalene building block in **i6**. The latter loses a hydrogen atom to the 18π-aromatic chrysene ($C_{18}H_{12}$, **p6**) molecule in an overall endoergic reaction (115 kJmol^{-1}) with respect to separated reactants. This reaction energy agrees well with the data obtained from Active Thermochemical Tables (ATcT) and NIST Chemistry Webbook (102 kJmol^{-1}). Chrysene belongs to the phenacenes, i.e. a class of PAHs characterized by a zigzag arrangement of fused benzene rings. An alternative pathway to **i5** and, eventually to **p6** via **i2**→**i13**→**i14**→**i5**→**i6**→**p6** also links to chrysene, but this high-energy mechanism requires overcoming an energetically unfavorable transition state located 401 kJmol^{-1} above the separated reactants.

Further, the spiro-intermediate **i4** also connects to [4]-helicene (**p4**, 136 kJmol^{-1}). Here, isomerization step of **i4** to **i9** carrying a fused three-membered ring needs to cross a barrier of 76 kJmol^{-1}; **i9** also represents a much higher energy intermediate (184 kJmol^{-1}) compared to any of the intermediates in the **i4**→**p6** (chrysene) pathway, where **i5** possesses the maximum energy of 132 kJmol^{-1}. A ring expansion from **i9** to **i10** occurs through a high energy transition state (190 kJmol^{-1} from the separated reactants) generating the carbon skeleton of [4]-helicene (**p4**) and hence four six-membered rings. Followed by the second hydrogen-atom loss, **i10** forms [4]-helicene (**p4**,

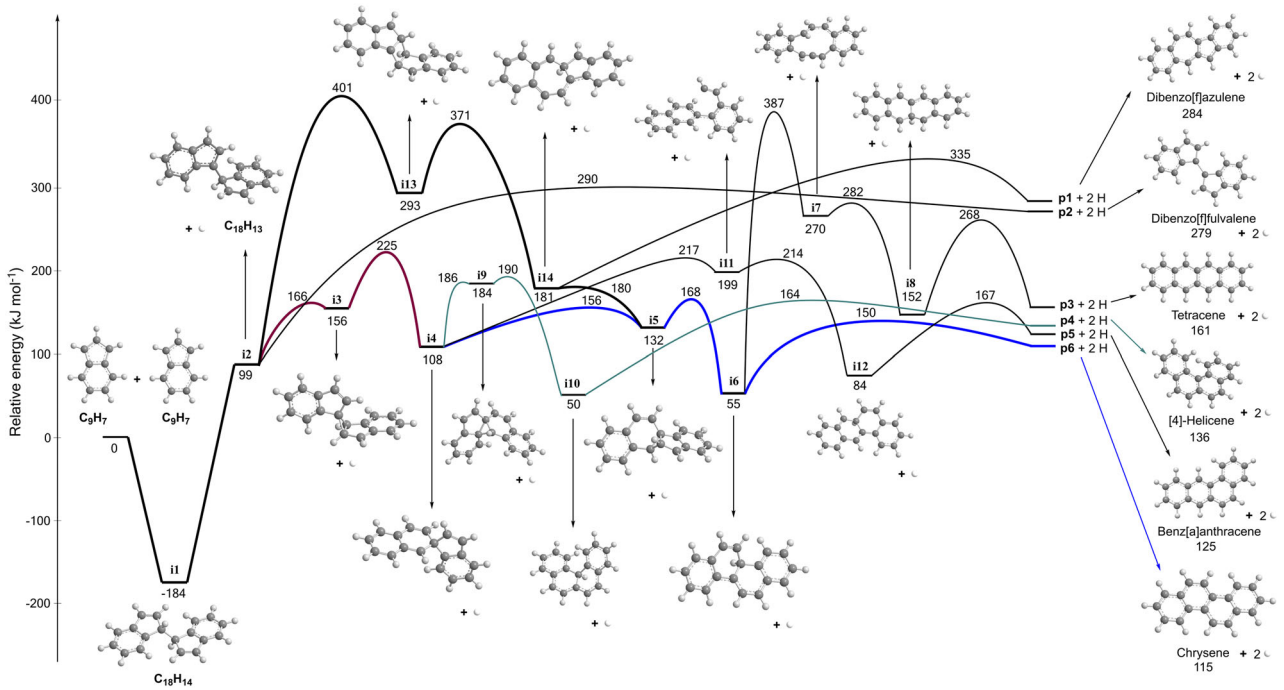

FIGURE 2 | Potential energy surface (PES) for the indenyl ($C_9H_7^{\bullet}$) self-reaction calculated at the G3(MP2, CC)//B3LYP/6-311G(d, p) level of theory leading to $C_{18}H_{12}$ products. Pathways to chrysene are highlighted by bold connecting lines.

136 kJmol^{-1}). This calculated endoergicity agrees well with the values from the Active Thermochemical Tables (ATcT) and the NIST Chemistry WebBook (126 kJmol^{-1}), indicating that our computed results are accurate within approximately ±10 kJmol^{-1}. The high energy intermediate **i9** and the associated transition states in the **i4→p4** pathway restrict the formation of [4]-helicene under the reaction conditions. The gas phase formation of benz[a]anthracene (**p5**) involves a ring-opening step via **i4→i11** along with the inherent large barrier of 217 kJmol^{-1} in the reaction sequence **i4→i11→i12→p5** which limits access to the generation of benz[a]anthracene (**p5**). This barrier also largely exceeds the highest energy transition state located at 168 kJmol^{-1} for the minimum energy pathway originating from **i4** yielding **p6**. Identical factors essentially hinder the formation of dibenzo[f]azulene (**p1**), dibenzo[f]fulvalene (**p2**) and tetracene (**p3**) involving transition states located at 401, 290 and 387 kJmol^{-1}, respectively. Essentially, our experimental findings are also supported by statistical computation utilizing Rice–Ramsperger–Kassel–Marcus (RRKM) – Master Equation (RRKM-ME) theory predicting dominant contribution of chrysene (**p6**, 87%) with smaller fractions of [4]-helicene (**p4**, 6%), benz[a]anthracene (**p5**, 5%) and dibenzo[f]fulvalene (**p2**, 2%) at our experimental temperature of 1223 ± 20 K (Figure 3). Rate constants for these products are also computed in the 0.1–10 atm range of pressures employing RRKM-ME theory that also reveals dominant chrysene formation (Figures S5–S7).

Wang et al. recently reported a mass growth process initiated by the 2-indenyl radical using a 420 mm reaction tube—over 20 times longer than the reactor exploited in the present study. The resulting residence times of several milliseconds, compared to some 100 μs here, enabled multistep reaction pathways and molecular mass growth beyond chrysene, which were the main focus of their work [41]. Wang et al. employed the MN15/MG3S density functional theory (DFT) method, whereas the present study used the higher-level G3(MP2, CC)// B3LYP/6–311G(d,p) approach, which achieves chemical accuracy within ±10 kJmol^{-1}, beyond the precision typically attainable by DFT. Notably, the potential energy surface (PES) reported by Wang et al. requires correction for the $H_2 \rightarrow 2H$ dissociation energy (432 kJmol^{-1}) [42], as their model considered hydrogen abstraction by free hydrogen atoms rather than unimolecular decomposition of reaction intermediates. In practice, unimolecular hydrogen atom loss and bimolecular hydrogen atom abstraction can compete, depending on temperature and the concentration of hydrogen atoms. Below we also extend our calculations to explore the effects of in situ generated atomic hydrogen that leads to highly exergonic reaction sequence along the indenyl self-reaction pathways.

We performed calculations of ΔG_r for individual reaction steps and the overall reaction for the formation of the observed products. Results of these calculations are illustrated in Figure 4. Figure 4a shows ΔG_r values for individual steps. One can see that the initial reaction step, $C_9H_7^{\bullet} + C_9H_7^{\bullet} \rightarrow C_{18}H_{13}^{\bullet}$ (**i2**) + H, is endergonic and its ΔG_r grows with temperature. At the highest temperature in the microreactor, ΔG_r for this step is about 163 kJmol^{-1} which corresponds to the equilibrium constant K_{equ} as low as ~10^{-7}. If we consider the stabilization-dissociation mechanism instead of well-skipping. i.e., $C_9H_7^{\bullet} + C_9H_7^{\bullet} \rightarrow C_{18}H_{14}$ (**i1**), followed by $C_{18}H_{14}$ (**i1**) → $C_{18}H_{13}^{\bullet}$ (**i2**) + H, the first step is exergonic up to 1000 K turning into endergonic at higher temperatures. However, **i1** can be readily stabilized (thermalized) collisionally at the microreactor's pressures and its reverse decomposition back to the reactants is slow, so that the equilibrium is unlikely to be achieved. Moreover, the $C_{18}H_{14}$ (**i1**) → $C_{18}H_{13}^{\bullet}$ (**i2**) + H decomposition channel is significantly slower than the reverse decomposition of **i1** to two indenyl radicals. Thus, $C_{18}H_{14}$ (**i1**) can persist in the microreactor, which is

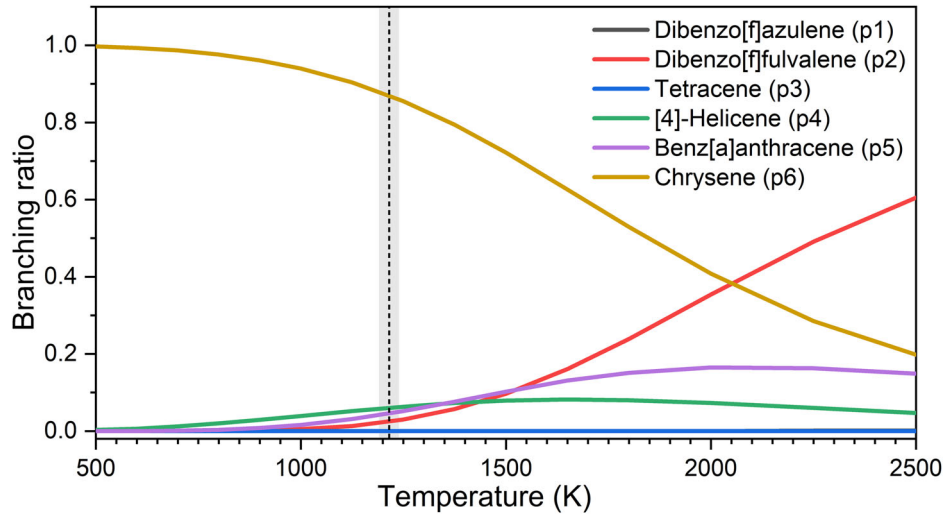

FIGURE 3 | Calculated branching ratios using the energetics in the PES for the formation of $C_{18}H_{12}$ products. The dotted line and the shaded region represent the experimental temperature (1223 K) and uncertainty range (±20 K), respectively.

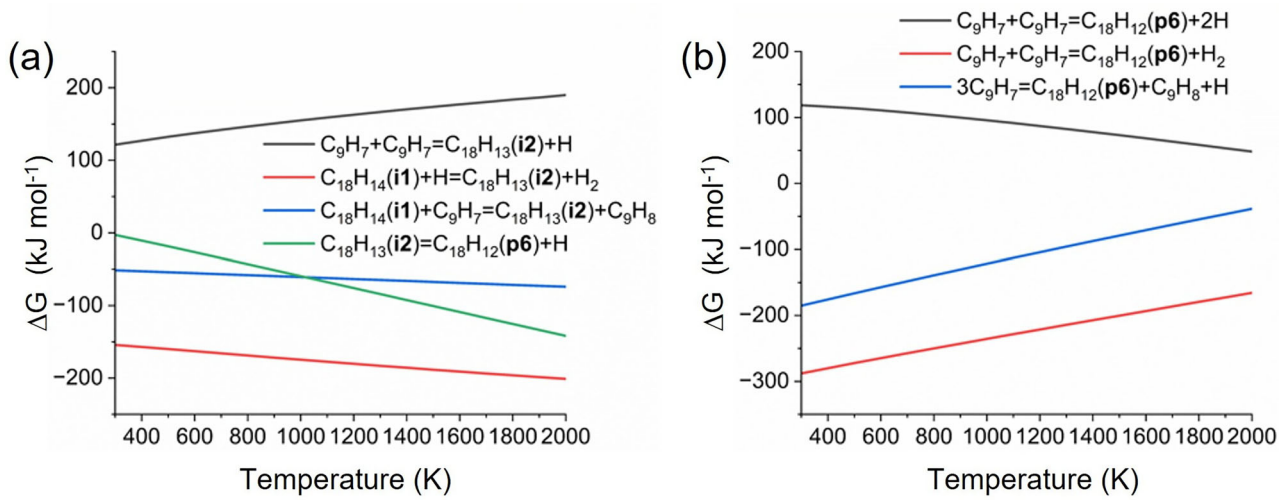

FIGURE 4 | Calculated reaction Gibbs energies for (a) the individual reaction steps and (b) the overall reaction for the conversion of two indenyl radicals to chrysene as functions of temperature.

supported by the detection of the m/z = 230 peak. When radicals such as H-atom, are present, they can abstract H-atoms from **i1** in a highly exergonic reaction $C_{18}H_{14}$ (**i1**) + H → $C_{18}H_{13}^{\bullet}$ (**i2**) + H_2 (see Figure 4a).

Another radical, which is abundant in the system and likely more abundant than H, is indenyl itself being the primary reactant, and the H-abstraction reaction, $C_{18}H_{14}$ (**i1**) + $C_9H_7^{\bullet}$ → $C_{18}H_{13}^{\bullet}$ (**i2**) + C_9H_8, is also significantly exergonic due to the weaker C—H bond breaking in **i1** than the forming C—H bond in indene. The feasibility of this reaction to occur is corroborated by the experimental observation of indene at m/z = 116 (Figure 1b). Once $C_{18}H_{13}^{\bullet}$ (**i2**) is produced, its reaction toward chrysene + H is exergonic, with ΔG_r rapidly decreasing with temperature. Considering the overall reaction process converting two indenyl radicals to chrysene, the $C_9H_7^{\bullet}$ + $C_9H_7^{\bullet}$ → $C_{18}H_{12}$ (**p6**) + 2H reaction is endergonic and thus thermodynamically unfavorable (Figure 4b). However, in the presence of H-radicals or with participation of an extra indenyl facilitating the formation of $C_{18}H_{13}^{\bullet}$ (**i2**), the $C_9H_7^{\bullet}$ + $C_9H_7^{\bullet}$ → $C_{18}H_{12}$ (**p6**) + H_2 and $3C_9H_7^{\bullet}$ → $C_{18}H_{12}$ (**p6**) + C_9H_8 + H reactions are exergonic, with the latter being less exergonic than the former. For instance, at the microreactor's temperature, $\Delta G_r[3C_9H_7^{\bullet} \rightarrow C_{18}H_{12}$ (**p6**) + C_9H_8 + H] is about −104 kJmol^{-1} but it grows with temperature to −39 kJmol^{-1} at 2000 K. Summarizing, the self-reaction of two indenyl radicals facilitated by participation of another indenyl appears to be the most plausible path for the observed formation of chrysene, along with indene and an H-atom.

In conclusion, this study provides clear evidence for the exclusive gas phase formation of the 18π Hückel-aromatic chrysene ($C_{18}H_{12}$)–the simplest representative of phenacenes—through the self-reaction of the 1-indenyl radical via spiroaromatic intermediates. The reactor conditions (pressure and temperature) were carefully optimized to limit further mass-growth processes, allowing us to isolate and investigate the fundamental reaction

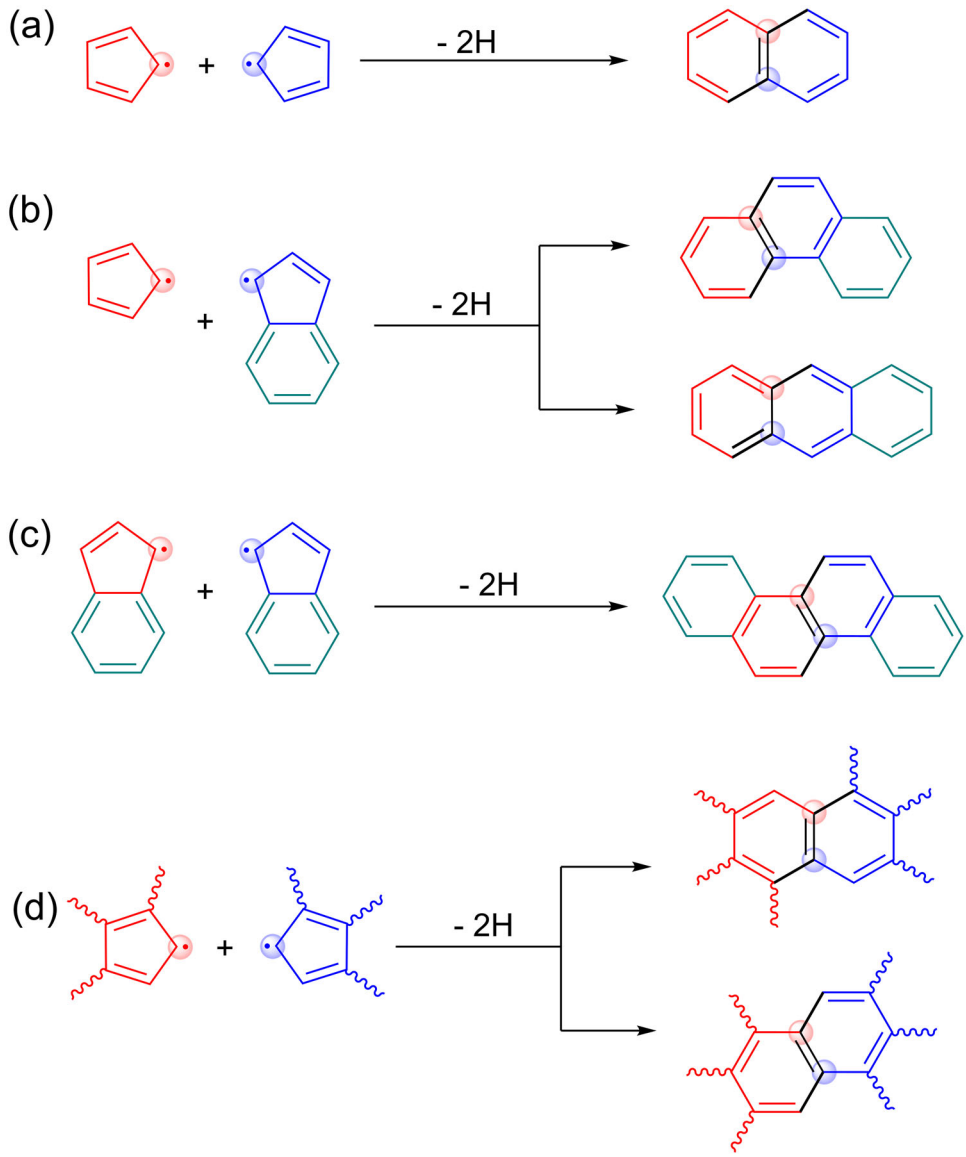

SCHEME 2 | Ring expansions originating from the cyclopentadienyl radical moiety in the recombination reactions of resonantly-stabilized free radicals—(a) cyclopentadienyl ($C_5H_5^{\bullet}$) self-reaction, (b) cyclopentadienyl ($C_5H_5^{\bullet}$) + 1-indenyl ($C_9H_7^{\bullet}$) reaction via C1 coupling, (c) 1-indenyl ($C_9H_7^{\bullet}$) self-reaction (C1-C1 coupling), and (d) generalized mechanistic outline for cyclopentadienyl addition-naphthylization (CPAN) leading to the preferred formation of benzenoid PAHs.

pathways between two 1-indenyl radicals. These findings uncover previously unknown mechanisms that initiate aromatic ring formation at high temperatures, offering new insights into the chemical processes occurring in circumstellar envelopes and the outflows of evolved carbon stars, such as IRC+10216, and their planetary nebula descendants [43, 44]. Here, the explored potential energy surface indicates solely *endoergic* pathways to chrysene under conditions replicating dying carbon-rich AGB stars. Even the highest transition states of 225 kJmol^{-1} identified in the dominating pathways to chrysene can be overcome close to the central star at temperatures of up to a few 1000 K, where chrysene was tentatively detected by mid infrared spectroscopy [45]. The non-detection of indene (C_9H_8) in circumstellar envelopes of carbon-rich stars might imply a rapid photolytic conversion to the 1-indenyl radical followed by a facile high temperature reaction to chrysene. In general, PAHs along with mass growth processes achieve significantly more stability and resistance to degradation by cosmic rays and thermal radiation [2]. The primary mass growth product in our study, chrysene has been also identified in carbonaceous chondrite meteorites, particularly Murchison, and recently in the asteroid Ryugu with laboratory analyses indicating that chrysene was part of the early solar system's organic inventory [5, 13, 46, 47]. These PAHs eventually survive to be delivered to molecular clouds and further incorporated into Solar System bodies as detected in meteorites and very recently on the carbonaceous asteroid Ryugu [45, 48, 49].

From the mechanistic viewpoint, the self-reaction of 1-indenyl radicals represents a versatile class of radical-radical reaction involving the formation of two six-membered rings originating from five-membered ring reactants that facilitate molecular mass growth processes (Scheme 2). For instance, the self-reaction of cyclopentadienyl ($C_5H_5^{\bullet}$) radical yields the simplest PAH with two benzene rings – naphthalene ($C_{10}H_8$) [50]. Based on

this radical-induced molecular mass growth mechanism, larger RSFRs such as the fluorenyl radical ($C_{13}H_9^{\bullet}$) are predicted to generate a PAH with six benzene rings ($C_{26}H_{16}$) upon self-reaction; in recombination with the 1-indenyl radical, this pathway may lead to PAHs carrying five benzene rings ($C_{22}H_{14}$). As a matter of fact, *any* PAH radical carrying a cyclopentadienyl radical moiety can recombine with yet another radical with a cyclopentadienyl radical moiety through this mechanism as sketched in Scheme 2.

It is important to note that a 1 nm soot particle–if the carbon is present in the form of aromatic units–carries about 50 carbon atoms. A nanoparticle with a cyclopentadienyl radical moiety can react readily with a cyclopentadienyl radical moiety in another nanoparticle leading to facile molecular mass growth processes aggregating to larger clusters via the cyclopentadienyl addition-naphthylization (CPAN) mechanism. Thus, this mechanistic pathway provides a versatile, high temperature formation route to larger PAHs, eventually leading to soot and carbonaceous grains in deep space and in combustion settings eventually delivered to carbonaceous asteroids and chondrites [4, 13, 51, 52].

Author Contributions

Souvick Biswas: conceptualization, methodology, investigation, writing – original draft, writing – review and editing, formal analysis, data curation, visualization, validation. **Shane J. Goettl:** data curation, investigation. **Vladislav S. Krasnoukhov:** methodology, formal analysis, investigation, data curation, software. **Nureshan Dias:** data curation. **Valeriy N. Azyazov:** investigation, methodology. **Sabrina Arias:** investigation, methodology. **Stanislaw F. Wnuk:** investigation, methodology, supervision. **Musahid Ahmed:** investigation, writing – review and editing, methodology, validation, resources. **Alexander M. Mebel:** conceptualization, investigation, writing – review and editing, methodology, validation, software. **Ralf I. Kaiser:** conceptualization, investigation, funding acquisition, writing – review and editing, visualization, validation, methodology, project administration, supervision, resources.

Acknowledgments

This work was supported by the US Department of Energy, Basic Energy Sciences DE-FG02-03ER15411, DE-AC02-05CH11231 (experimental studies). Nureshan Dias and Musahid Ahmed were supported by the Director, Office of Science, Office of Basic Energy Sciences, of the US Department of Energy under Contract No. DE-AC02-05CH11231, through the Gas Phase Chemical Physics program of the Chemical Sciences Division. The Advanced Light Source at Berkeley is also supported under Contract No. DE-AC02-05CH11231.

Conflicts of Interest

The authors declare no conflicts of interest.

Data Availability Statement

The data that support the findings of this study are available from the corresponding author upon reasonable request.

References

1. C. M. J. A. Walmsley, "Identification of the "Unidentified IR Features" of Interstellar Dust," *Astronomy and Astrophysics* 500 (2009): 281–283, https://doi.org/10.1051/0004-6361/200912164.

2. A. G. G. M. Tielens, "The Molecular Universe," *Review of Modern Physics* 85 (2013): 1021–1081, https://doi.org/10.1103/RevModPhys.85.1021.

3. W. W. Duley, "Polycyclic Aromatic Hydrocarbons, Carbon Nanoparticles and the Diffuse Interstellar Bands," *Faraday Discussions* 133 (2006): 415–425, https://doi.org/10.1039/b516323d.

4. H. Sabbah, G. Quitté, K. Demyk, and C. Joblin, "First Direct Detection of Large Polycyclic Aromatic Hydrocarbons On Asteroid (162173) Ryugu Samples: An Interstellar Heritage," *Natural Science* 4 (2024): e20240010.

5. J. C. Aponte, J. P. Dworkin, D. P. Glavin, et al., "PAHs, Hydrocarbons, and Dimethylsulfides in Asteroid Ryugu Samples A0106 and C0107 and the Orgueil (CI1) Meteorite," *Earth Planets Space* 75 (2023): 28, https://doi.org/10.1186/s40623-022-01758-4.

6. S. Tachibana, H. Sawada, R. Okazaki, et al., "Pebbles and Sand on Asteroid (162173) Ryugu: In Situ Observation and Particles Returned to Earth," *Science* 375 (2022): 1011–1016, https://doi.org/10.1126/science.abj8624.

7. J. C. Gradie, C. R. Chapman, and E. F. Tedesco, "Distribution of Taxonomic Classes and the Compositional Structure of the Asteroid Belt," *In Asteroids* II (1989): 316–335.

8. J. R. Cronin, S. Pizzarello, and D. P. Cruikshank, "*Organic Matter in Carbonaceous Chondrites, Planetary Satellites, Asteroids and Comets*," (University of Arizona Press, 1988), 819–857.

9. M. Lecasble, L. Remusat, J.-C. Viennet, B. Laurent, and S. Bernard, "Polycyclic Aromatic Hydrocarbons in Carbonaceous Chondrites Can be Used as Tracers of both Pre-accretion and Secondary Processes," *Geochimica et Cosmochimica Acta* 335 (2022): 243–255, https://doi.org/10.1016/j.gca.2022.08.039.

10. M. Saito and Y. Kimura, "Origin of Organic Globules in Meteorites: Laboratory Simulation Using Aromatic Hydrocarbons," *The Astrophysical Journal* 703 (2009): L147, https://doi.org/10.1088/0004-637X/703/2/L147.

11. L. Remusat, F. Robert, A. Meibom, et al., "Proto-Planetary Disk Chemistry Recorded by D-Rich Organic Radicals in Carbonaceous Chondrites," *The Astrophysical Journal* 698 (2009): 2087, https://doi.org/10.1088/0004-637X/698/2/2087.

12. L. Remusat, Y. Guan, Y. Wang, and J. M. Eiler, "Accretion and Preservation of D-Rich Organic Particles in Carbonaceous Chondrites: Evidence for Important Transport in the Early Solar System Nebula," *The Astrophysical Journal* 713 (2010): 1048, https://doi.org/10.1088/0004-637X/713/2/1048.

13. S. S. Zeichner, J. C. Aponte, S. Bhattacharjee, et al., "Polycyclic Aromatic Hydrocarbons in Samples of Ryugu Formed in the Interstellar Medium," *Science* 382 (2023): 1411–1416, https://doi.org/10.1126/science.adg6304.

14. Y. Wang, Y. Huang, C. M. O. D. Alexander, M. Fogel, and G. Cody, "Molecular and Compound-specific Hydrogen Isotope Analyses of Insoluble Organic Matter From Different Carbonaceous Chondrite Groups," *Geochimica et Cosmochimica Acta* 69 (2005): 3711–3721, https://doi.org/10.1016/j.gca.2005.03.008.

15. R. Zenobi, J.-M. Philippoz, R. N. Zare, and P. R. Buseck, "Spatially Resolved Organic Analysis of the Allende Meteorite," *Science* 246 (1989): 1026–1029, https://doi.org/10.1126/science.246.4933.1026.

16. A. G. G. M. Tielens, "Interstellar Polycyclic Aromatic Hydrocarbon Molecules," *Annual Review of Astronomy and Astrophysics* 46 (2008): 289–337, https://doi.org/10.1146/annurev.astro.46.060407.145211.

17. M. Frenklach, "Reaction Mechanism of Soot Formation in Flames," *Physical Chemistry Chemical Physics* 4 (2002): 2028–2037, https://doi.org/10.1039/b110045a.

18. E. Micelotta, A. Jones, and A. J. A. Tielens, "Polycyclic Aromatic Hydrocarbon Processing in Interstellar Shocks," *Astronomy and Astrophysics* 510 (2010): A36, https://doi.org/10.1051/0004-6361/200911682.

19. K. Johansson, M. Head-Gordon, P. Schrader, K. Wilson, and H. J. S. Michelsen, "Resonance-stabilized Hydrocarbon-radical Chain Reactions

May Explain Soot Inception and Growth," *Science* 361 (2018): 997–1000, https://doi.org/10.1126/science.aat3417.

20. V. D. Knyazev and K. V. Popov, "Kinetics of the Self Reaction of Cyclopentadienyl Radicals," *The Journal of Physical Chemistry A* 119 (2015): 7418–7429, https://doi.org/10.1021/acs.jpca.5b00644.

21. L. Zhao, R. I. Kaiser, W. Lu, et al., "Molecular Mass Growth Through Ring Expansion in Polycyclic Aromatic Hydrocarbons via Radical–Radical Reactions," *Nature Communications* 10 (2019): 3689, https://doi.org/10.1038/s41467-019-11652-5.

22. V. S. Krasnoukhov, M. V. Zagidullin, I. P. Zavershinskiy, and A. M. Mebel, "Formation of Phenanthrene via Recombination of Indenyl and Cyclopentadienyl Radicals: A Theoretical Study," *The Journal of Physical Chemistry A* 124 (2020): 9933–9941, https://doi.org/10.1021/acs.jpca.0c09091.

23. S. Sinha, R. K. Rahman, and A. Raj, "On the Role of Resonantly Stabilized Radicals in Polycyclic Aromatic Hydrocarbon (PAH) Formation: Pyrene and Fluoranthene Formation From Benzyl–Indenyl Addition," *Physical Chemistry Chemical Physics* 19 (2017): 19262–19278, https://doi.org/10.1039/C7CP02539D.

24. L. Zhao, R. I. Kaiser, W. Lu, et al., "A Free-Radical Prompted Barrierless Gas-Phase Synthesis of Pentacene," *Angewandte Chemie, International Edition* 59 (2020): 11334–11338, https://doi.org/10.1002/anie.202003402.

25. L. Zhao, R. I. Kaiser, B. Xu, et al., "A Unified Mechanism on the Formation of Acenes, Helicenes, and Phenacenes in the Gas Phase," *Angewandte Chemie, International Edition* 59 (2020): 4051–4058, https://doi.org/10.1002/anie.201913037.

26. Z. Yang, G. R. Galimova, C. He, et al., "Gas-phase Formation of the Resonantly Stabilized 1-Indenyl ($C_9H_7^{\bullet}$) Radical in the Interstellar Medium," *Science Advances* 9 (2023): eadi5060, https://doi.org/10.1126/sciadv.adi5060.

27. C. He, R. I. Kaiser, W. Lu, et al., "Exotic Reaction Dynamics in the Gas-Phase Preparation of Anthracene ($C_{14}H_{10}$) via Spiroaromatic Radical Transients in the Indenyl–Cyclopentadienyl Radical–Radical Reaction," *Journal of the American Chemical Society* 145 (2023): 3084–3091, https://doi.org/10.1021/jacs.2c12045.

28. S. Doddipatla, G. R. Galimova, H. Wei, et al., "Low-temperature Gas-phase Formation of Indene in the Interstellar Medium," *Science Advances* 7 (2021): eabd4044, https://doi.org/10.1126/sciadv.abd4044.

29. S. J. Goettl, M. Ahmed, A. M. Mebel, and R. I. Kaiser, "Molecular Mass Growth Processes to Polycyclic Aromatic Hydrocarbons Through Radical–Radical Reactions Exploiting Photoionization Reflectron Time-of-Flight Mass Spectrometry," *Accounts of Chemical Research* 58 (2025): 2682–2694, https://doi.org/10.1021/acs.accounts.5c00311.

30. L. Zhao, M. B. Prendergast, R. I. Kaiser, et al., "Reactivity of the Indenyl Radical (C_9H_7) With Acetylene (C_2H_2) and Vinylacetylene (C_4H_4)," *ChemPhysChem* 20 (2019): 1437–1447, https://doi.org/10.1002/cphc.201900052.

31. S. Biswas, J. Cokas, W. Gee, et al., "Unconventional Low Temperature Decomposition of a Saturated Hydrocarbon Over Atomically-dispersed Titanium-aluminum-boron Catalyst," *Nature Communications* 16 (2025): 6793, https://doi.org/10.1038/s41467-025-62112-2.

32. S. Biswas, D. Paul, N. Dias, et al., "Efficient Oxidative Decomposition of Jet-Fuel Exo -Tetrahydrodicyclopentadiene (JP-10) by Aluminum Nanoparticles in a Catalytic Microreactor: An Online Vacuum Ultraviolet Photoionization Study," *The Journal of Physical Chemistry A* 128 (2024): 1665–1684, https://doi.org/10.1021/acs.jpca.3c08125.

33. H. Jin, J. Yang, L. Xing, et al., "An Experimental Study of Indene Pyrolysis With Synchrotron Vacuum Ultraviolet Photoionization Mass Spectrometry," *Physical Chemistry Chemical Physics* 21 (2019): 5510–5520, https://doi.org/10.1039/C8CP07285J.

34. R. I. Kaiser and N. Hansen, "An Aromatic Universe–A Physical Chemistry Perspective," *The Journal of Physical Chemistry A* 125 (2021): 3826–3840, https://doi.org/10.1021/acs.jpca.1c00606.

35. R. I. Kaiser, O. Asvany, and Y. T. Lee, "Crossed Beam Investigation of Elementary Reactions Relevant to the Formation of Polycyclic Aromatic Hydrocarbon (PAH)-Like Molecules in Extraterrestrial Environments," *Planetary and Space Science* 48 (2000): 483–492, https://doi.org/10.1016/S0032-0633(00)00021-0.

36. M. V. Zagidullin, R. I. Kaiser, D. P. Porfiriev, et al., "Functional Relationships Between Kinetic, Flow, and Geometrical Parameters in a High-Temperature Chemical Microreactor," *The Journal of Physical Chemistry A* 122 (2018): 8819–8827, https://doi.org/10.1021/acs.jpca.8b06837.

37. C. Wentrup, H.-W. Winter, and D. Kvaskoff, "C_9H_8 Pyrolysis. *o*-Tolylacetylene, Indene, 1-Indenyl, and Biindenyls and the Mechanism of Indene Pyrolysis," *The Journal of Physical Chemistry A* 119 (2015): 6370–6376, https://doi.org/10.1021/acs.jpca.5b03453.

38. A. M. Mebel, A. Landera, and R. I. Kaiser, "Formation Mechanisms of Naphthalene and Indene: From the Interstellar Medium to Combustion Flames," *The Journal of Physical Chemistry A* 121 (2017): 901–926, https://doi.org/10.1021/acs.jpca.6b09735.

39. F. Zhang, R. I. Kaiser, V. V. Kislov, A. M. Mebel, A. Golan, and M. Ahmed, "A VUV Photoionization Study of the Formation of the Indene Molecule and Its Isomers," *The Journal of Physical Chemistry Letters* 2 (2011): 1731–1735, https://doi.org/10.1021/jz200715u.

40. D. S. N. Parker, F. Zhang, R. I. Kaiser, V. V. Kislov, and A. M. Mebel, "Indene Formation Under Single-Collision Conditions From the Reaction of Phenyl Radicals With Allene and Methylacetylene—A Crossed Molecular Beam and Ab Initio Study," *Chemistry - An Asian Journal* 6 (2011): 3035–3047, https://doi.org/10.1002/asia.201100535.

41. H. Wang, J. Guan, J. Gao, et al., "Direct Observation of Covalently Bound Clusters in Resonantly Stabilized Radical Reactions and Implications for Carbonaceous Particle Growth," *Journal of the American Chemical Society* 146 (2024): 13571–13579, https://doi.org/10.1021/jacs.4c03417.

42. B. Ruscic, R. E. Pinzon, M. L. Morton, et al., "Introduction to Active Thermochemical Tables: Several "Key" Enthalpies of Formation Revisited," *The Journal of Physical Chemistry A* 108 (2004): 9979–9997, https://doi.org/10.1021/jp047912y.

43. L. M. Ziurys, "The Chemistry in Circumstellar Envelopes of Evolved Stars: Following the Origin of the Elements to the Origin of Life," *Proceedings of the National Academy of Sciences of the United States of America* 103 (2006): 12274–12279, https://doi.org/10.1073/pnas.0602277103.

44. E. Lagadec, D. Mékarnia, J. A. F. Pacheco, and C. J. A. Dougados, "Dust Temperature and Density Profiles in the Envelopes of AGB and Post-AGB Carbon Stars From Mid-infrared Observations," *Astronomy and Astrophysics* 433 (2005): 553–564, https://doi.org/10.1051/0004-6361:20041553.

45. K. Justtanont, M. Barlow, C. Skinner, P. Roche, D. Aitken, and C. J. A. Smith, "Mid-infrared Spectroscopy of Carbon-Rich Post-AGB Objects and Detection of the PAH Molecule Chrysene," *Astronomy and Astrophysics* 309 (1996): 612–628.

46. M. A. Sephton, G. D. Love, J. S. Watson, et al., "Hydropyrolysis of Insoluble Carbonaceous Matter in the Murchison Meteorite: New Insights Into Its Macromolecular Structure," *Geochimica et Cosmochimica Acta* 68 (2004): 1385–1393, https://doi.org/10.1016/j.gca.2003.08.019.

47. M. P. Callahan, A. Abo-Riziq, B. Crews, L. Grace, and M. S. de Vries, "Isomer Discrimination of Polycyclic Aromatic Hydrocarbons in the Murchison Meteorite by Resonant Ionization," *Spectrochimica Acta Part A: Molecular and Biomolecular Spectroscopy* 71 (2008): 1492–1495, https://doi.org/10.1016/j.saa.2008.05.005.

48. K. K. Larsen, M. Schiller, and M. Bizzarro, "Accretion Timescales and Style of Asteroidal Differentiation in an 26Al-poor Protoplanetary Disk," *Geochimica et Cosmochimica Acta* 176 (2016): 295–315, https://doi.org/10.1016/j.gca.2015.10.036.

49. M. Frenklach and E. D. Feigelson, "Formation of Polycyclic Aromatic Hydrocarbons in Circumstellar Envelopes," *The Astrophysical Journal* 341 (1989): 372, https://doi.org/10.1086/167501.

50. R. I. Kaiser, L. Zhao, W. Lu, et al., "Formation of Benzene and Naphthalene Through Cyclopentadienyl-Mediated Radical–Radical Reactions," *The Journal of Physical Chemistry Letters* 13 (2022): 208–213, https://doi.org/10.1021/acs.jpclett.1c03733.

51. S. Mostefaoui, P. Hoppe, and A. El Goresy, "In Situ Discovery of Graphite With Interstellar Isotopic Signatures in a Chondrule-Free Clast in an L3 Chondrite," *Science* 280 (1998): 1418–1420, https://doi.org/10.1126/science.280.5368.1418.

52. E. Zinner, S. Amari, B. Wopenka, and R. S. Lewis, "Interstellar Graphite in Meteorites: Isotopic Compositions and Structural Properties of Single Graphite Grains From Murchison," *Meteoritics* 30 (1995): 209–226, https://doi.org/10.1111/j.1945-5100.1995.tb01115.x.

53. F. Qi, "Combustion Chemistry Probed by Synchrotron VUV Photoionization Mass Spectrometry," *Proceedings of the Combustion Institute* 34 (2013): 33–63, https://doi.org/10.1016/j.proci.2012.09.002.

54. A. G. Baboul, L. A. Curtiss, P. C. Redfern, and K. Raghavachari, "Gaussian-3 Theory Using Density Functional Geometries and Zero-point Energies," *Journal of Chemical Physics* 110 (1999): 7650–7657, https://doi.org/10.1063/1.478676.

55. L. A. Curtiss, K. Raghavachari, P. C. Redfern, A. G. Baboul, and J. A. Pople, "Gaussian-3 Theory Using Coupled Cluster Energies," *Chemical Physics Letters* 314 (1999): 101–107, https://doi.org/10.1016/S0009-2614(99)01126-4.

56. L. A. Curtiss, K. Raghavachari, P. C. Redfern, V. Rassolov, and J. A. Pople, "Gaussian-3 (G3) Theory for Molecules Containing First and Second-row Atoms," *Journal of Chemical Physics* 109 (1998): 7764–7776, https://doi.org/10.1063/1.477422.

57. M. J. T. Frisch, H. B. Schlegel, G. E. Scuseria, et al., *Gaussian 09, Revision D.01*, (Gaussian, Inc, 2009).

58. H.-J. Werner and P. J. Knowles, *MOLPRO, Version 2015.1, a Package of Ab Initio Programs* (University College Cardiff Consultants Ltd, 2015).

59. V. S. Krasnoukhov, M. V. Zagidullin, V. N. Azyazov, and A. M. Mebel, "Mechanism of Formation of Four-Ring Polycyclic Aromatic Hydrocarbons in the Self-Recombination of Indenyl," *Combust Explos Shock Waves* 59 (2023): 151–158, https://doi.org/10.1134/S0010508223020053.

60. Y. Georgievskii, J. A. Miller, M. P. Burke, and S. J. Klippenstein, "Reformulation and Solution of the Master Equation for Multiple-Well Chemical Reactions," *The Journal of Physical Chemistry A* 117 (2013): 12146–12154, https://doi.org/10.1021/jp4060704.

61. Y. Georgievskii and S. J. Klippenstein, "MESS.2016.3.23".

62. J. Troe, "Theory of Thermal Unimolecular Reactions at Low Pressures. I. Solutions of the Master Equation," *Journal of Chemical Physics* 66 (1977): 4745–4757, https://doi.org/10.1063/1.433837.

Supporting Information

Additional supporting information can be found online in the Supporting Information section.

Supporting File 1: The authors have cited additional references within the Supporting Information [53–62].